The release of air bubbles from an underwater nozzle

By MICHAEL S. LONGUET-HIGGINS[1],
BRYAN R. KERMAN[2] AND KNUD LUNDE[3]

[1] Institute for Nonlinear Science, University of California, San Diego, La Jolla, CA 92093, USA

[2] Canada Centre for Inland Waters, Burlington, Ontario L7R 4AL, Canada

[3] Department of Applied Mathematics and Theoretical Physics, Silver Street,
Cambridge CB3 9EW, UK

Air bubbles released from an underwater nozzle emit an acoustical pulse which is of interest both for the study of bubble detachment and for elucidating the mechanism of sound generation by a newly formed bubble. In this paper we calculate theoretically the sequence of bubble shapes from a given nozzle and show that there is for each nozzle a bubble of maximum volume V_{max}. Assuming that the bubble becomes detached at its 'neck', and that the volume of the detached bubble equals the volume V^* of the undetached bubble above its 'neck', we determine for each nozzle diameter D an acoustic frequency f^* corresponding to 'slow' bubble release.

Experiments show that the acoustic frequency, hence the bubble size, depends on the rate of air flow to the bubble, but for slow rates of flow the frequency f is very close to the theoretical frequency f^*.

High-speed photographs suggest that when the bubble pinches off, the limiting form of the surface is almost a cone. This is accounted for by assuming a line sink along the axis of symmetry. Immediately following pinch-off there is evidence of the formation of an axial jet going upwards into the bubble. This may play a part in stimulating the emission of sound.

1. Introduction

An apparently very simple source of underwater sound is the release of an air bubble from an underwater nozzle, as in the classical experiments of Minnaert (1933). While Minnaert used only his ear to determine the pitch of the sound, an instrumental record of the pressure together with a sequence of photographs was published by Strasberg (1956); see also Fitzpatrick & Strasberg (1957). Because of the controllable nature of the source, such data are of considerable interest for a discussion of the mechanics of sound generation by bubbles (Longuet-Higgins 1989 *a*, *b*, 1990 *a*), whether they arise from waterfalls (Leighton & Walton 1987), breaking waves (Farmer & Vagle 1988), bubble splitting (Frizell & Arndt 1987), raindrops (Prosperetti, Crum & Pumphrey 1989) or other causes.

Longuet-Higgins (1989 *a*, *b*, 1990 *a*) suggested that the monopole emission of sound by shape oscillations in newly generated bubbles could make an appreciable contribution to the oceanic acoustical noise spectrum. The mechanism involves a damped 'resonance' between the shape oscillations (at second order) and the radial 'breathing' mode of the bubble. An attempt to test this idea by a laboratory

experiment was suggested by L. A. Crum and A. Prosperetti (personal communication). They proposed measuring the sound from the bubbles released from an underwater nozzle, over a range of different ambient pressures. As we shall see, however, this experiment needs to be conducted with due regard to the rate of air flow into the bubble, and other factors.

The sound emitted from bubbles entrained by falling drops has been the subject of recent studies by Prosperetti *et al.* (1989), Longuet-Higgins (1990*b*) and Oğuz & Prosperetti (1991). Although here the problem is complicated by the presence of a free surface nearby, the situation may not be unlike the problem of bubble detachment from a nozzle. The same remark applies to the sound from bubbles trapped by capillary–gravity waves on water (see Longuet-Higgins 1990*a*).

The forms of bubbles emerging from an underwater nozzle are similar in principle to those of drops hanging from a vertical tube, in that both are governed by the known equations for a meniscus (see Bashforth & Adams 1883; Padday 1971). Only the contact angles are different in the two cases, leading generally to different solutions. With a theoretically thin-walled tube or nozzle, however, the solutions become identical. The stability of pendant drops has been studied theoretically by Padday & Pitt (1972); see also Michael (1981). It appears that in the simplest situation when the volume of the bubble (as opposed to the air pressure) is controlled experimentally, the question of stability is relatively straightforward. Nevertheless the present authors have not been able to find a satisfactory account of the subject relating to bubbles from a nozzle, even in this simplest case.

Another application should be mentioned here. In studying the behaviour of air bubbles released from a nozzle, it is desirable to have some simple and accurate method for sizing the bubbles. For this purpose, the frequency of the acoustical pulse emitted by the bubble, which is simply related to its radius, may be the most accurate indicator of its size, and more convenient than flash photography.

In the present paper we shall solve the problem of the growth of air bubbles from an underwater nozzle from first principles, but treating only the case when the air flow is small, so that the situation is quasi-steady. For each nozzle-size we find a bubble shape of maximum volume, which cannot be exceeded while maintaining stability. We assume that the bubble breaks off at this point, at the narrowest point of its profile. This gives a theoretical air volume and bubble radius, hence an acoustical frequency (figure 15). It turns out that this accurately corresponds to a maximum acoustical frequency measured in our experiments on the gentle release of bubbles from an underwater nozzle (see §8).

High-speed photographs of the bubble profiles (figure 19) confirm the sequence of theoretical bubble profiles up to the point of maximum volume. They also yield information on the subsequent velocity field, which will be of value in calculating theoretically the magnitude of the acoustical signal due to different mechanisms.

2. Static meniscus

Consider the static problem of an air bubble emerging from a vertical tube, as in figure 1, at a rate slow enough that the fluid velocities may be neglected. The free surface is then in equilibrium under the action of surface tension T and gravity g. If ρ denotes the density of the surrounding water we can choose units so that

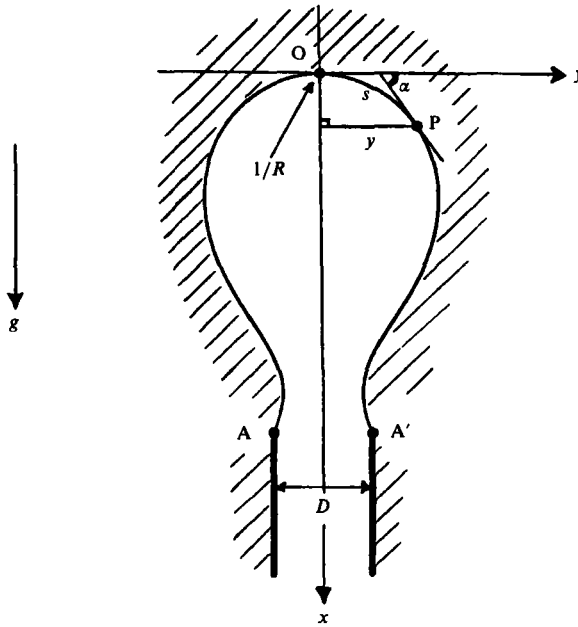$$g = 1, \quad \rho = 1, \quad T = 1. \tag{2.1}$$

FIGURE 1. Coordinates and axes for a bubble emerging from an underwater nozzle.

This implies that the unit of length is

$$(T/\rho g)^{\frac{1}{2}} = 2.75 \text{ mm}. \tag{2.2}$$

Choose coordinates as in figure 1 with the origin O at the highest point of the meniscus, the x-axis as the axis of symmetry, and the y-axis radially outwards. The pressure p in the fluid is given by

$$p = p_0 + x, \tag{2.3}$$

where p_0 is the pressure at O. The air pressure p_B in the bubble is given by

$$p_B = p + (\kappa_1 + \kappa_2), \tag{2.4}$$

where κ_1 and κ_2 are the principal curvatures of the surface. If s denotes the arclength from O to a point P on the surface, and if α denotes the angle made by the tangent at P with the horizontal, then we have

$$\kappa_1 = \frac{d\alpha}{ds}, \quad \kappa_2 = \frac{\sin\alpha}{y}. \tag{2.5}$$

Note that as $s \to 0$, we have

$$\kappa_1 \to \frac{1}{R}, \quad \kappa_2 \to \frac{1}{R} \tag{2.6}$$

where R denotes the radius of curvature at O. Clearly from (2.4)

$$p_B = p_0 + \frac{2}{R} \tag{2.7}$$

and from (2.3) to (2.7) we have in general

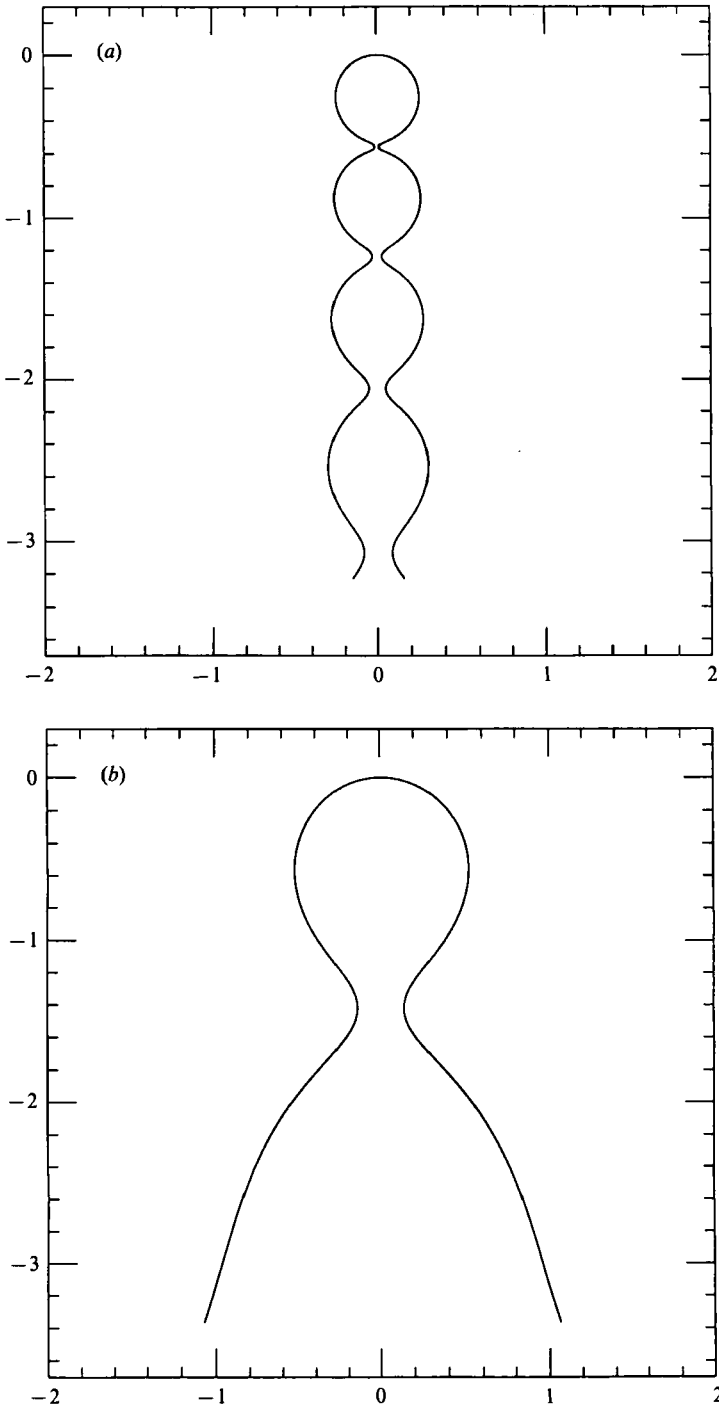$$\frac{d\alpha}{ds} + \frac{\sin\alpha}{y} = \frac{2}{R} - x, \tag{2.8}$$

FIGURE 2(*a,b*). For caption see facing page.
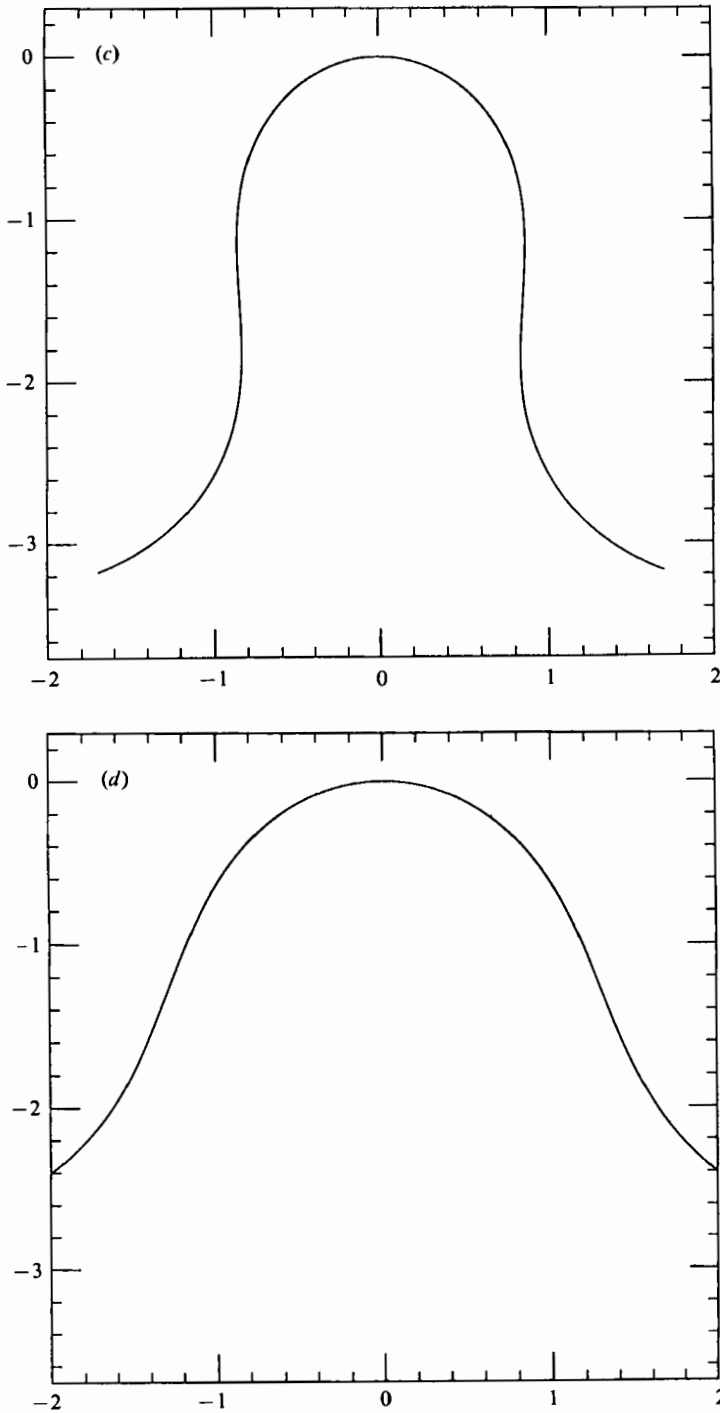
FIGURE 2. Solutions of equations (2.8) and (2.9) representing bubble menisci. (a) $R = 0.25$, (b) $R = 0.50$, (c) $R = 0.75$, (d) $R = 1.00$.
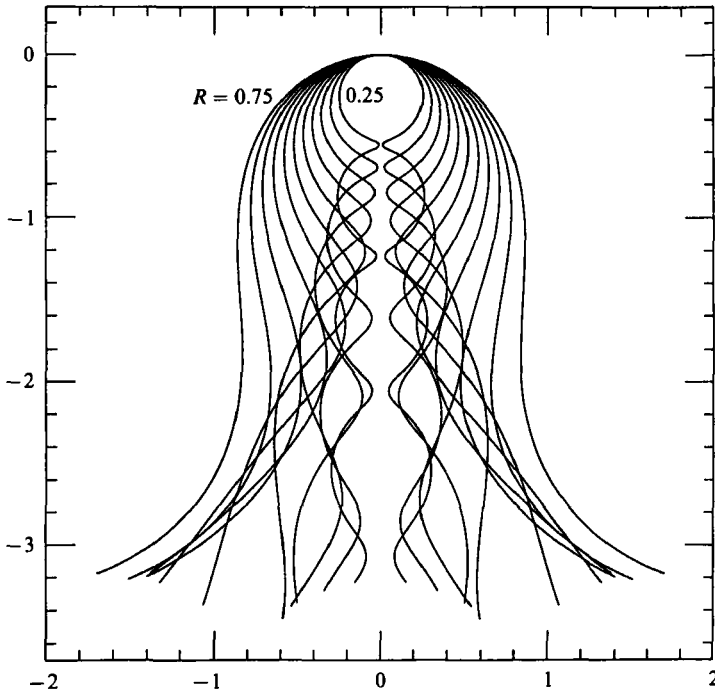
FIGURE 3. Family of solutions of equations (2.8) and (2.9), $R = 0.25$–0.75.

with
$$x = \int_0^s \sin\alpha\,\mathrm{d}s, \qquad y = \int_0^s \cos\alpha\,\mathrm{d}s. \tag{2.9}$$

These equations can be accurately integrated by noting that

$$\frac{\mathrm{d}\alpha}{\mathrm{d}s} = \frac{2}{R} - x - \frac{\sin\alpha}{y}, \tag{2.10}$$

hence
$$\frac{\mathrm{d}^2\alpha}{\mathrm{d}s^2} = -\sin\alpha - \frac{\cos\alpha}{y}\left(\frac{\mathrm{d}\alpha}{\mathrm{d}s} - \frac{\sin\alpha}{y}\right), \tag{2.11}$$

and then using the numerical scheme described by Pitts (1974, equations (A 11)–(A 15)).

Figure 2(*a–d*) shows some representative solutions, corresponding to $R = 0.25$, 0.50, 0.75 and 1.0 respectively. The family of solutions, from $R = 0.25$ to 0.75 is shown in figure 3. We note that this type of presentation differs from the more usual one given for example by Padday (1971, figure 10) in which the curvature at $x = 0$ is held constant and the parameter $\beta = \rho g R^2/T$ is varied. In the present treatment the physical scale is held constant throughout.

3. The case $R \ll 1$

For small values of R the effect of gravity is slight compared to that of surface tension. The profiles in figures 2 and 3 then resemble the surfaces of Delaunay (1841), of which some examples are shown in figure 4. These surfaces are by definition the
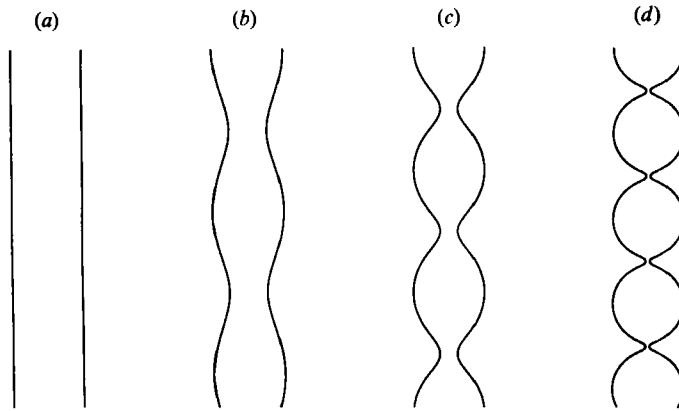
Figure 4. Delaunay surfaces: solutions of equation (3.1). (a) $C = 0.50$, (b) $C = 0.65$, (c) $C = 0.80$, (d) $C = 0.95$.

periodic, axisymmetric surfaces having constant mean curvature. The axial sections are thus solutions of the equation

$$\frac{\mathrm{d}\alpha}{\mathrm{d}s} + \frac{\sin\alpha}{y} = 2C. \tag{3.1}$$

In Cartesian coordinates the solutions can be expressed in terms of elliptic functions, and it is curious that each curve may be obtained as the locus of the focus of an ellipse that rolls without slipping along a straight line, the axis of symmetry (see also Eells 1987). Clearly when the rolling ellipse is a circle, its focus traces out a straight line. On the other hand when the ellipse is very thin, with a focus near each end, the focus traces circles very nearly, as in figure 4 (*d*).

Note that near the point of greatest distance y from the axis of symmetry the two principal curvatures κ_1 and κ_2 are of the same sign and almost equal to C. Near the point of minimum y, however, κ_1 and κ_2 are of opposite sign and both large; only their sum equals $2C$.

Without gravity, there is no characteristic lengthscale. Physically the surfaces are unstable unless anchored by two parallel rings separated by not more than one wavelength (Plateau 1873).

As seen in figure 2(*a*), the addition of a small axial component of gravity causes the surfaces to develop a sequence of widening 'necks'. The width d of the first neck is easily calculated. For, since the surface above the neck is almost a sphere of radius R, its volume is $\frac{4}{3}\pi R^3$. Consider the equilibrium of the part of the surface above the neck (as argued by Blanchard & Syzdek (1977) who, however, consider only small bubbles). The buoyancy of the sphere must be balanced by the surface tension at the neck, which gives a force πd, in dimensionless units. Hence

$$d = \tfrac{4}{3}R^3. \tag{3.2}$$

The argument can obviously be generalized to show that the diameter of the nth 'neck' in the series is $\frac{4}{3}nR^3$, so long as the n successive segments of the surface remain nearly spherical.

For larger values of R the surfaces in figure 2 broaden out more rapidly, and the number of minimum values of y for each surface is less. At the critical value

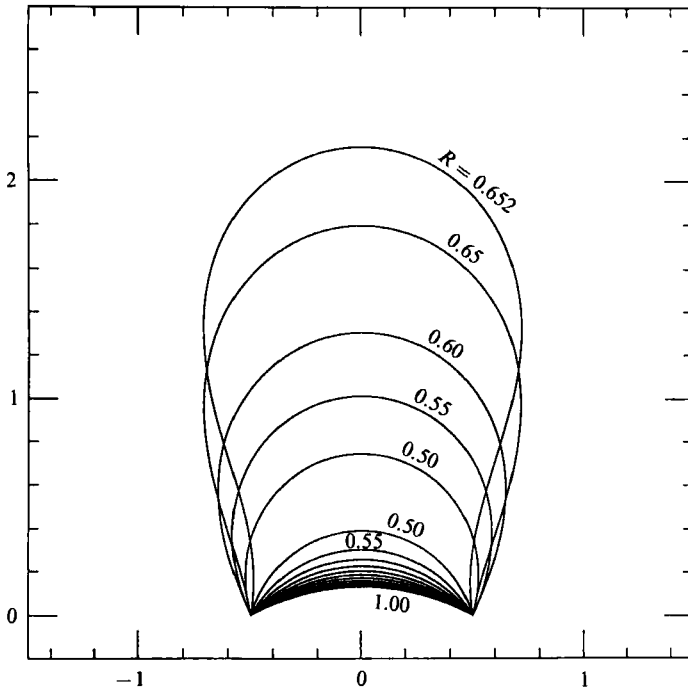$$R = R_{\mathrm{crit}} = 0.7788 \tag{3.3}$$

FIGURE 5. Successive bubble profiles emerging from a nozzle of diameter $D = 1.0$
(dimensionless units).

the surface loses its last minimum, i.e. the tangent at the point of inflection of the
profile becomes vertical. The corresponding value of the radial distance y is

$$y_{\text{crit}} = 0.897. \tag{3.4}$$

4. Sequence of bubble shapes

Consider a bubble emerging from a thin-walled nozzle as in figure 1. The effect of
assuming the wall to be thin is that the bubble attachment can occur at any angle
α to the rim of the nozzle. To determine the sequence of shapes corresponding to a
nozzle of given diameter D we have to take the intersection of the lines $y = \pm 0.5D$
with the family of profiles in figure 3. At a given R the line $y = 0.5D$ will intersect the
profile at one or more points with coordinates $(x_m, 0.5D)$, say, numbered in order of
increasing x_m.

For illustration consider the sequence of bubble shapes in a typical case $D = 1.0$
(figure 5). As R decreases from 1.0 to a little less than 0.5, the volume steadily
increases until the tangent at the nozzle rim becomes vertical. Near this point there
is a sharp increase in volume with little accompanying change in R. The solution
switches from x_1 to x_2, and V increases steadily as x_2 and R increase. This continues
until $R = 0.655$ when the tangent at the neck again becomes vertical, and there is
another sharp increase in V; x_2 then changes to x_3, and R decreases. Shortly
afterwards, at $R = 0.652$, the volume attains a maximum. If further air is forced in,
the bubble must break off.

The volume
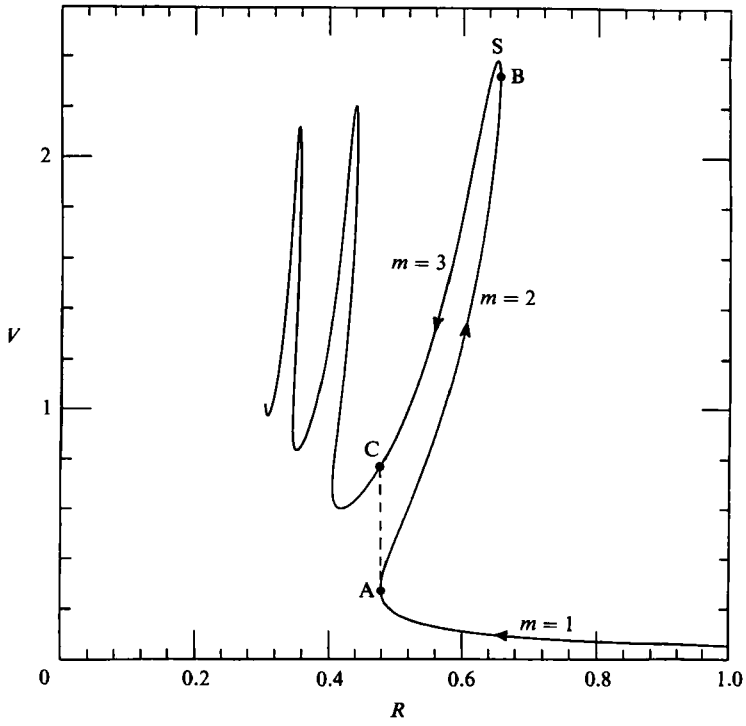
$$V = \pi \int_0^{x_m} y^2 \, \mathrm{d}x \tag{4.1}$$

FIGURE 6. The volume V enclosed above the rim of a nozzle of diameter $D = 1.0$, as a function of the radius of curvature R.
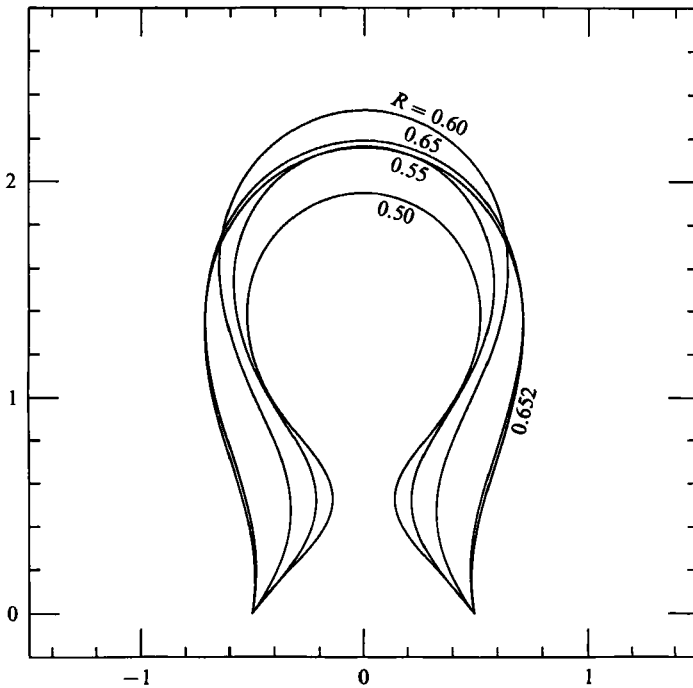

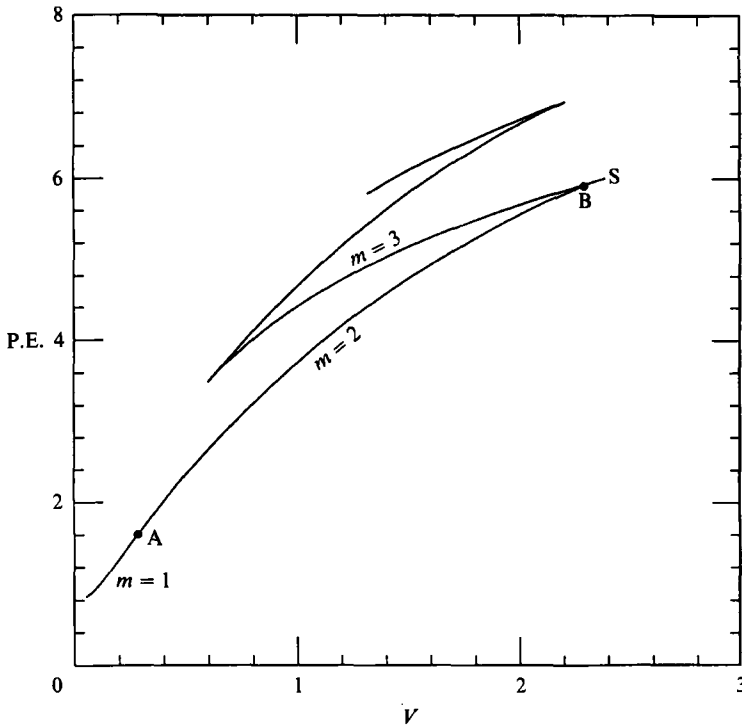FIGURE 7. The sequence of bubble profiles corresponding to $m = 3$, when $D = 1.0$.

FIGURE 8. Potential energy corresponding to bubble profiles in sequences $m = 1$, 2 and 3, when $D = 1.0$.

of air contained in the bubble above the level of the nozzle rim is plotted as a function of R in figure 6. The different branches x_m are identified. Physically the parameter moves along the branch $m = 1$ until the point A. Then, if the bubble shape evolves continuously, it moves up the branch $m = 2$ as far as B, where it passes over to $m = 3$.

In figure 7 we show the profiles of the bubbles along the branch $m = 3$. Each of these has a narrow neck, but with a volume V less than the maximum. Physically it is conceivable that with the aid of a small perturbation a bubble might jump from the branch $m = 2$ to the branch $m = 3$. However, a calculation of the potential energy (surface tension plus gravitational) of the bubbles shows that, at equal volume V, the potential energy of bubbles on branch $m = 3$ is greater (see figure 8). Hence some energy would need to be supplied.

If we follow the behaviour of V to the left of the line AC in figure 6 we find a repetition of the previous behaviour. However, the points in this region correspond to profiles having more than one vertical tangent. It seems unlikely that these represent stable configurations, and they will not be discussed further.

5. Limiting bubbles

The family of curves of V versus R for different nozzle diameters is shown in figure 9. It will be seen that when

$$D < 2y_{\mathrm{crit}} = 1.794 \tag{5.1}$$

the curves have two critical tangents, as already discussed, but when $D > 2y_{\mathrm{crit}}$ there
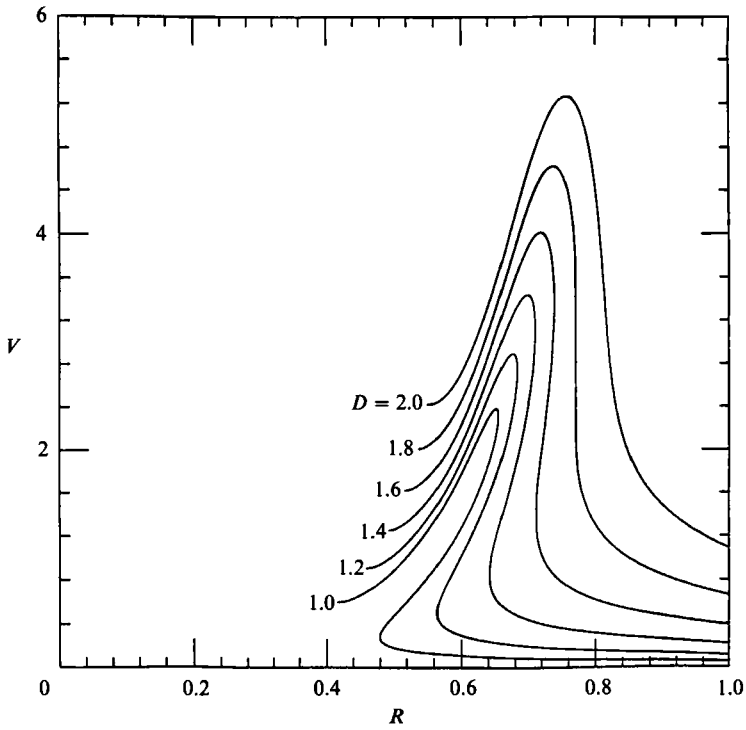
FIGURE 9. The volume V enclosed above the nozzle rim as a function of R for $D = 1.0$, 1.2, 1.4, 1.6, 1.8 and 2.0.

D	V_{max}	R	V^*	a^*	f (kHz)
0.2	0.530	0.460	0.530	0.502	2.490
0.4	0.991	0.540	0.987	0.618	2.023
0.6	1.444	0.589	1.437	0.700	1.786
0.8	1.905	0.624	1.867	0.764	1.636
1.0	2.387	0.652	2.270	0.815	1.534
1.2	2.897	0.677	2.650	0.858	1.457
1.4	3.439	0.698	2.954	0.890	1.404
1.5	3.723	0.709	3.096	0.904	1.372
1.6	4.014	0.718	3.200	0.914	1.368
1.7	4.314	0.729	3.305	0.924	1.342
1.8	4.624	0.739	3.376	0.931	1.343
1.9	4.939	0.746	3.405	0.933	1.340
2.0	5.260	0.761	3.395	0.932	1.331
2.1	5.598	0.767	3.357	0.929	1.346
2.2	5.938	0.776	3.107	0.905	1.381
2.3	6.283	0.788			
2.4	6.642	0.789			

TABLE 1. The maximum volume V_{max} of a bubble attached to a nozzle of diameter D. The unit of length is $(T/\rho g)^{\frac{1}{2}}$
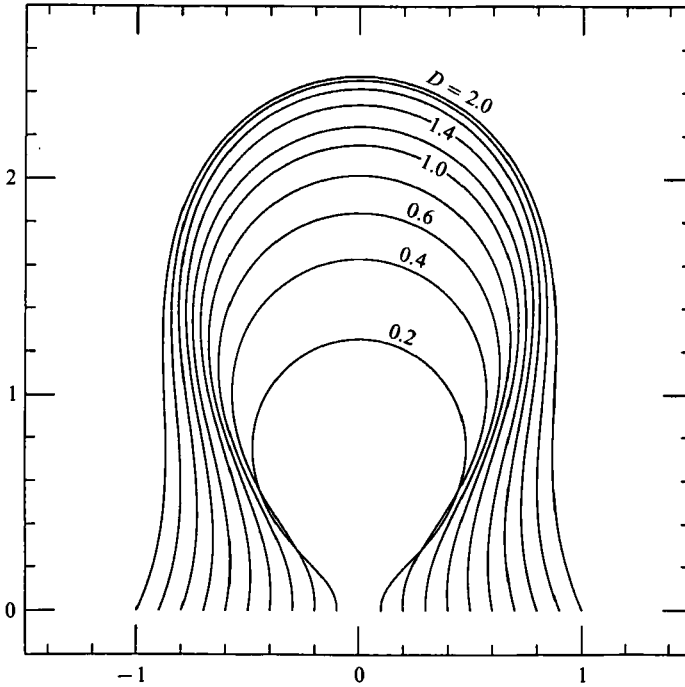
FIGURE 10. Limiting bubble profiles for nozzles of diameter D ranging from 0.2 to 2.0.

are none. In all cases, however, there is a maximum volume V_{max} corresponding to a nozzle of given diameter. Some representative values are given in table 1, together with the corresponding values of R.

The family of limiting bubble shapes is shown in figure 10 over the range $0.2 \leqslant D \leqslant 2.0$. When $D \leqslant 0.1$ the shape is almost a sphere with radius R. Since D then differs little from the neck width d, one can find R from (3.2), that is

$$R = (\tfrac{3}{4}D)^{\frac{1}{3}}. \tag{5.2}$$

6. Bubble release

The stability of a bubble attached to a nozzle has been discussed by Pitts (1974) under conditions of prescribed volume and of prescribed air pressure. We shall consider only the case of prescribed volume. We also assume that the rate at which air is passed into the bubble is small enough that the bubble can be considered to be in a static state, until the onset of instability.

If the bubble contains the maximum amount of air for the nozzle diameter, and further air is forced or allowed to enter, then it has no choice but to break off. Supposing the bubble has a thin 'neck' it is reasonable to suppose that the water surrounding the neck moves inwards towards the axis of symmetry and that the bubble thus breaks in a symmetrical fashion. What specially concerns us, for the emission of sound, is the total volume of the bubble after its release. We shall suppose that the total air mass M corresponds to the volume V^* of air above the level of the 'neck', where the diameter is equal to d. Generally V^* is less than V_{max} as we have seen. In figure 11, the parameter R is plotted against D, using the data in table 1. (The broken line shows the asymptote (5.2).) Clearly R increases monotonically with D.
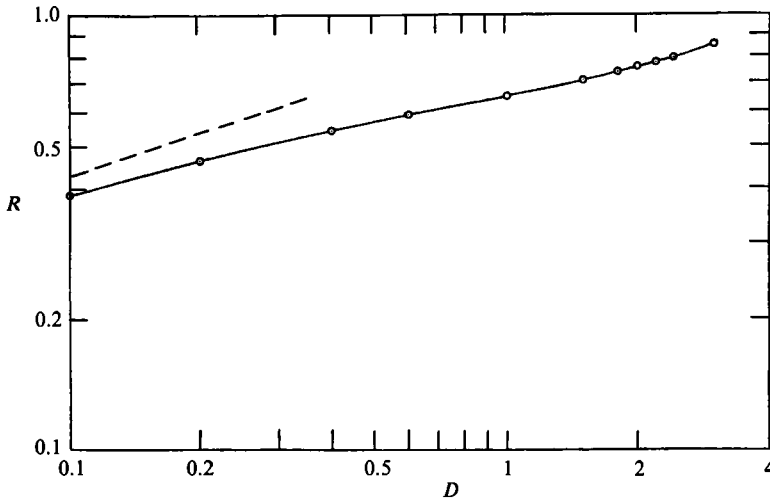
FIGURE 11. The value of R for limiting bubbles shown as a function of the nozzle diameter D. The broken line shows the asymptote (5.2).

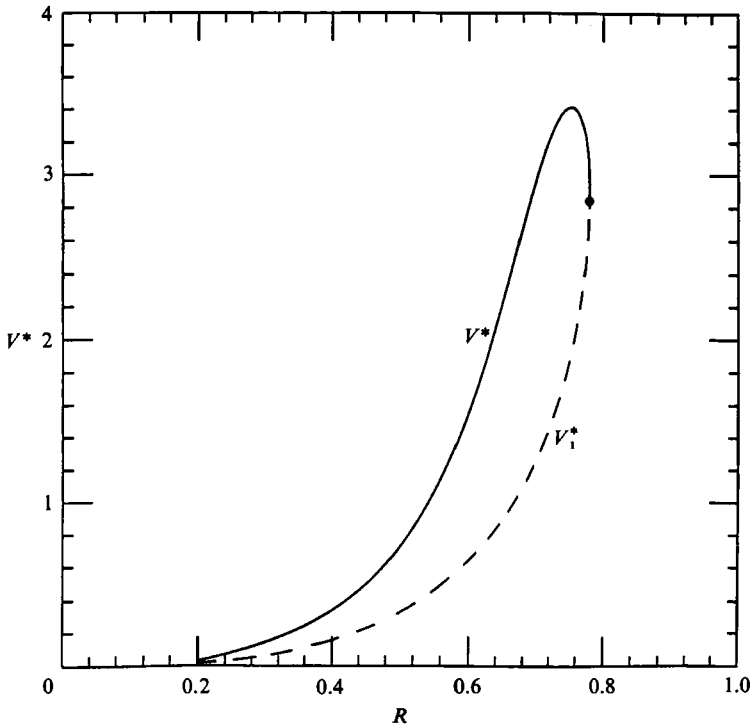

FIGURE 12. The dimensionless volume V^* contained above the 'neck' of a bubble, as a function of the radius of curvature R.

In figure 12, on the other hand, V^* is shown as a function of R. Clearly V^* is not a monotonic function of R since although the family of curves in figure 10 enclose one another, as R approaches R_{crit} (equation (3.3)) the neck of the curve moves rapidly upwards, so tending to reduce V^*. Indeed V^* must merge smoothly with V_1^*, the volume above the widest point of the profile, V_1^* is shown by the broken curve in figure 12.
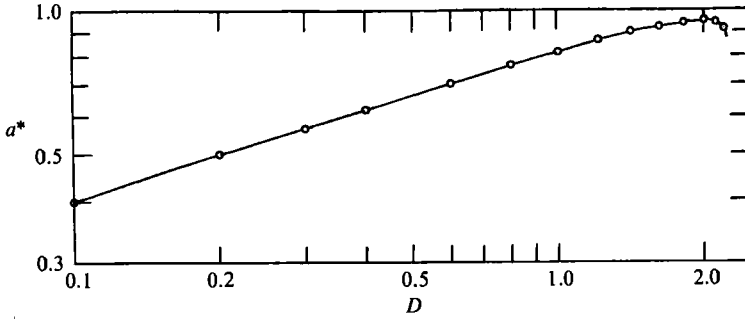
FIGURE 13. The notional radius a^* of limiting bubbles as a function of the nozzle diameter D.

Combining figures 11 and 12 we show in figure 13 the 'notional' radius a^* of the detached bubble, calculated from

$$a^* = (3V^*/4\pi)^{\frac{1}{3}}, \qquad (6.1)$$

as a function of the nozzle diameter D. We note that this is a non-monotonic function of D. In fact V^* has a maximum at about $R = 0.754$ where $V^* = 3.416$, $a^* = 0.9031$ and $D = 1.98$. The neck of the bubble finally disappears when $R = 0.7788$, $V^* = 2.875$, $a^* = 0.8284$ and $D = 2.25$.

7. Frequency of oscillation

The actual radius a' of a bubble immediately after its release will differ from the 'notional' radius a^* by an amount depending upon the environmental conditions. Let p_A denote the pressure in the water at a point immediately above the highest point of the bubble (see figure 14). Just before its release the pressure p_B in the bubble is then given by

$$p_B = p_A + 2T/R. \qquad (7.1)$$

Denoting by primes the corresponding quantities for the equilibrium state of the bubble immediately after its release, we have

$$p'_B = p'_A + 2T/a'. \qquad (7.2)$$

We may assume that $p'_A = p_A$. Also, from the gas law we have

$$p'_B/p_B = (V^*/V') = (a^*/a')^{3\gamma}, \qquad (7.3)$$

where γ lies between 1 and 1.4, depending on the bubble size. From the above relations it follows that

$$\frac{a'}{a^*} = \left(\frac{1+2T/pR}{1+2T/pa'}\right)^{\frac{1}{3\gamma}}. \qquad (7.4)$$

Now, for air bubbles of radius greater than 0.1 mm in water at atmospheric pressure, $2T/pa$ is less than 1%. So from (7.4) we have

$$\frac{a'}{a^*} = 1 + \epsilon\left(\frac{a^*}{R} - \frac{a^*}{a'}\right), \qquad (7.5)$$

where $\epsilon = (2T/3\gamma pa^*)$ is at most 0.003. Thus, to lowest order in ϵ,

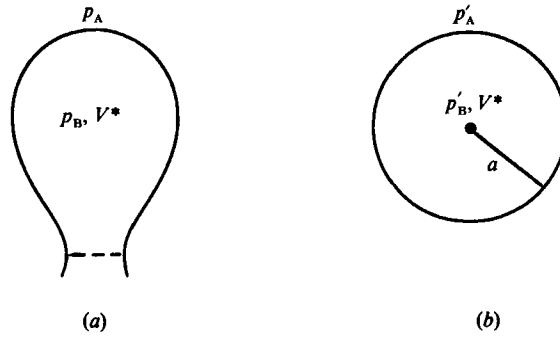$$\frac{a'}{a^*} = 1 + \delta, \qquad (7.6)$$

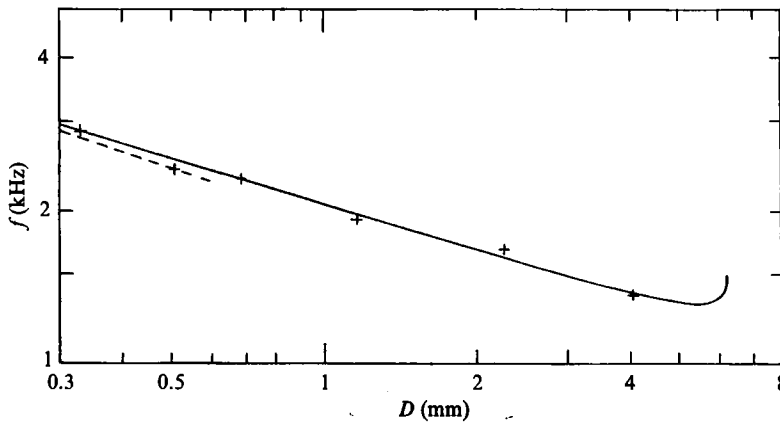FIGURE 14. Schematic drawing of a bubble (a) before and (b) after detachment.

FIGURE 15. The maximum acoustical frequency f of bubble oscillations as a function of nozzle diameter D. Solid line: from equation (7.11). Broken line: asymptote (7.12). Plotted points: experimental values (§8).

where
$$\delta = \epsilon\left(\frac{a^*}{R} - 1\right). \tag{7.7}$$

The ratio a^*/R is a measure of the distortion of the bubble, and is of order unity. Hence δ is a small quantity which we shall neglect.

The frequency f of the linear, radial oscillations of a bubble of radius a is given by

$$(2\pi f)^2 = \frac{3\gamma p_B}{\rho a^2} - \frac{2T}{\rho a^3} \tag{7.8}$$

(Plesset & Prosperetti 1977). Since the ratio of the second term on the right to the first term is $\epsilon/3\gamma$, the second term is negligible. For a similar reason p_B can be replaced by p_A, which we take to be the static pressure at a depth of 1 m below a water surface at sea level:

$$p_A = 1.11 \times 10^6 \text{ dyne/cm}^2. \tag{7.9}$$

Taking $\gamma = 1.4$ this yields

$$f = \frac{344}{a} \text{ Hz} \tag{7.10}$$

Nozzle number	ID (mm)	OD (mm)	Cross-section	f_{max} (kHz)
1	4.004	4.978	Sharp	1.368
2	2.286	2.972	Sharp	1.680
3	1.168	1.651	Sharp	1.944
4	0.686	1.092	Square	2.310
5	0.508	0.813	Square	2.420
6	0.330	0.635	Square	2.880

TABLE 2. Dimensions of underwater nozzles, and the observed maximum bubble frequencies

provided a is in cm. If a is in the dimensionless units of figure 13 ($1 \sim 0.275$ cm) then

$$f = \frac{1.250}{a^*} \text{ kHz}. \tag{7.11}$$

This quantity is shown in the last column of table 1, and is plotted in figure 15, as a function of the nozzle diameter D.

At small bubble radii, (3.2) yields the asymptote

$$f \propto D^{-\frac{1}{3}} \tag{7.12}$$

shown by the broken line in figure 15.

The frequency has a minimum value of 1.38 kHz when $D = 5.45$ mm, and a cutoff value 1.51 kHz when $D = 6.19$ mm.

8. Comparison with observation

A series of controlled experiments, in which air bubbles were released from a variety of nozzles at a depth of about 72 cm below a free water surface, were carried out in the Department of Applied Mathematics and Theoretical Physics at Cambridge University. A full account of the experimental arrangement is given by Lunde (1991).

The nozzles were placed near the bottom of a tank with horizontal cross-section 10 cm × 10 cm, the thickness of the Perspex wall being 0.95 cm ($\frac{3}{8}$ in.). The internal diameters of the nozzles ranged from 0.330 mm to 4.004 mm (see table 2). The source of air to the nozzles was a reservoir of compressed air, released through a micrometer-controlled valve, which enabled the rate of bubble production to be varied from 0.01 to 5 bubbles per second.

To ensure repeatability of the experiments the nozzle orifices were carefully prepared. The three largest nozzles in table 2 were shaped so that the inner edge was sharp, as seen in figure 19. The three smallest nozzles were square-topped.

A hydrophone was introduced to record the acoustical signal emitted on the release of each bubble. A typical pulse is shown in figure 16(a). It has the familiar form of a damped sine-wave (cf. Strasberg 1956). (The signal was digitized at 132 kHz and band-passed between 0.7 and 7.0 kHz.)

Figure 16(b) shows a frequency analysis of figure 16(a). There is clearly a well-defined peak frequency, which we can take as representative of the pulse.

As expected from Clift, Grace & Weber (1978) two important controlling factors were the rate of air flow to the bubble and whether the system operated in a pressure-
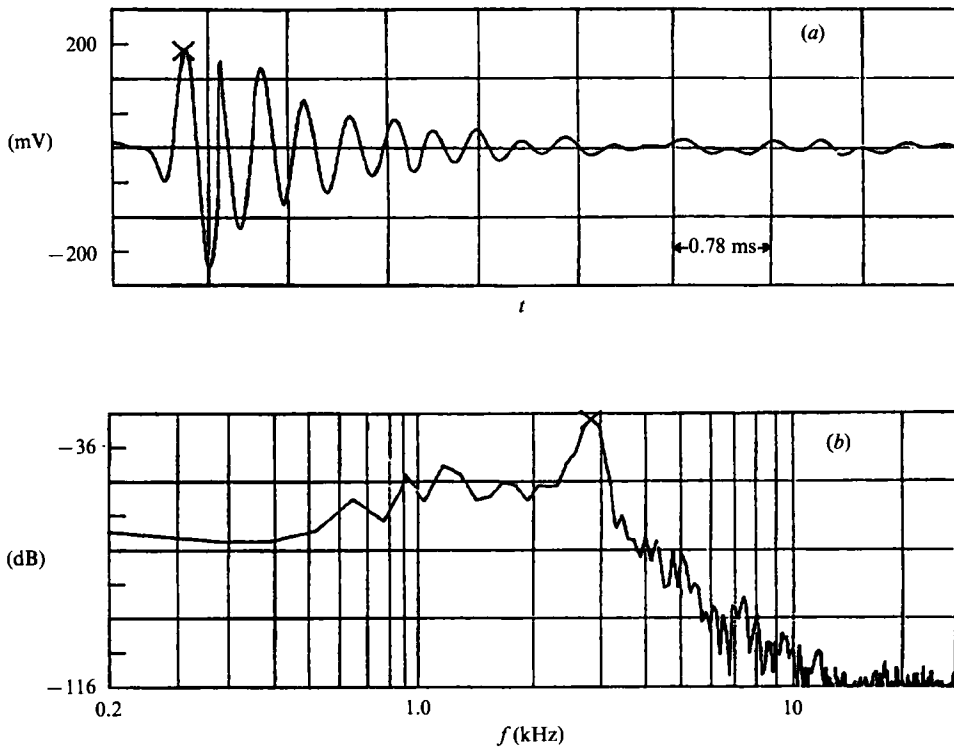
FIGURE 16. Acoustical pulse from a bubble released from Nozzle 6 at low air-flow rate.
(a) Time variation of the acoustical pressure, (b) frequency spectrum.

controlled or volume-controlled mode. Which mode was active depended on the volume of air between the nozzle and the flow control valve. If this volume was large compared to the bubble volume, then the bubble released was pressure-controlled, while if it was small, then the release was volume-controlled. An example is shown in figure 17 for Nozzle 3, where the initial amplitude of the pulse and the peak frequency are plotted as functions of the time interval between bubble release. In both cases the air supply lead contained the main volume of air between the nozzle and the control valve. In pressure-controlled release the lead between the nozzle and the control valve was 3 m long and had an ID of 4 mm. For volume-controlled release the lead was reduced to 0.1 m length and an ID of 2 mm. It will be noticed that in the case of volume-controlled release the variation of both amplitude and frequency is more gradual, and there apparently exist limiting values corresponding to long time-intervals, that is for 'gentle' release of the air bubbles.

Figure 18 (a) shows the peak frequency as a function of the release interval, for the six different nozzles, when the air leads were shortened as far as possible. Figure 18 (b) shows the normalized amplitudes, that is each amplitude divided by its least-observed value. This suggests that for the three largest nozzles the conditions were effectively volume-controlled, whereas for Nozzles 4 and 5, and possibly also 6, it was still partly pressure-controlled.

The observed peak frequencies for gentle release are given in table 2 and have been plotted (as crosses) in figure 15. It will be seen that they lie fairly well along the theoretical curve. Some possible sources of error are discussed in Appendices A and B.
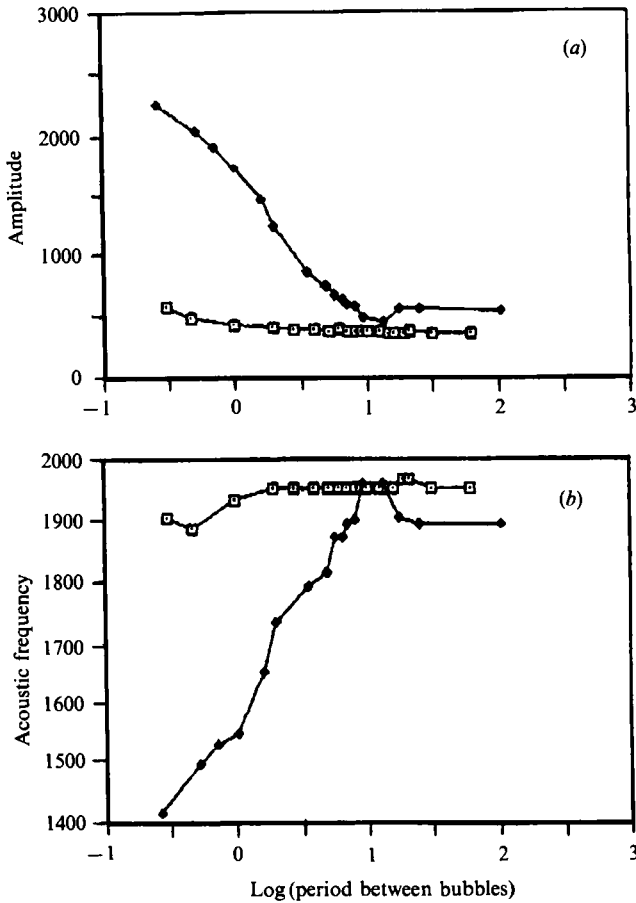
FIGURE 17. Dependence of acoustical pulse parameters on air-flow rate for Nozzle 3. (*a*) Peak-to-peak amplitude, (*b*) peak frequency. —□—, Volume-controlled release; —◆—, pressure controlled release.

The magnitude of the source was determined by placing the hydrophone at different distances x from the nozzle. For distances exceeding 2 cm the pulse amplitude was found to be strongly affected by the presence of the sidewalls, as expected. Near the nozzle, we might expect dipole behaviour owing to the presence of a pressure-release surface between the water and the air in the nozzle. By measurement it was found that the pressure amplitude behaved asymptotically like r^{-1}, indicating a source with dipole moment 0.45 ± 0.10 N/m. This value is of the same order of magnitude (0.3–0.4 N/m) as the acoustical pulse from bubbles typically entrained by short surface waves (Updegraff 1989; Medwin & Beaky 1989) and by rain-drops (0.3 to 0.8 N/m; see Prosperetti *et al.* 1989; Longuet-Higgins 1990). It is however less than the value of 2.3 N/m reported by Strasberg (1956) which may have been measured at a higher air flow rate.

9. Bubble profiles

Figure 19 shows frames from a high-speed film of bubbles emerging from Nozzle 1 at the rate of about one bubble per s. The dimensionless diameter D for this nozzle is 1.456.
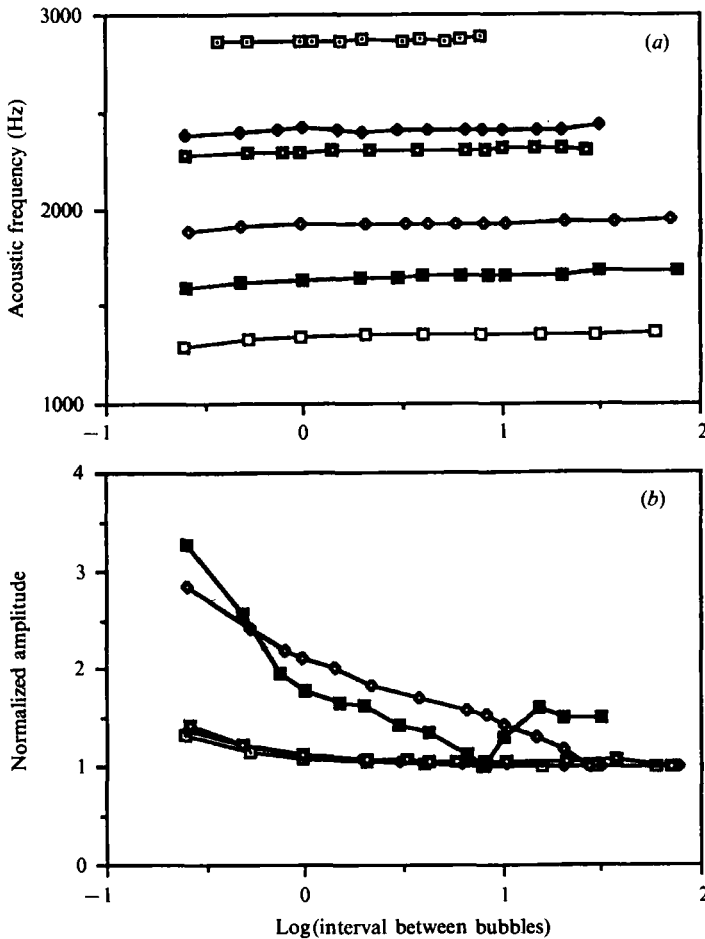
FIGURE 18. (*a*) Acoustic frequency as a function of release interval for the nozzles in table 2. (*b*) Peak-to-peak amplitude (normalized) as a function of release interval (except Nozzle 6).

To test the constancy of the flow rate we shown in figure 20 the theoretical sequence of bubble profiles for this nozzle at equal increments 0.2 of bubble volume, up to $V = 3.4$, together with the limiting bubble, $V = 3.597$. The height H of each bubble is plotted against its volume in figure 21. At first H increases linearly with V, then less rapidly on account of the greater bubble width, then finally more rapidly again, to compensate for the contraction in width at the neck of the bubble. The result is the S-shaped curve shown in figure 21.

Figure 22 shows the measured height of the bubbles (plotted points) taken from the photographs, as a function of the time t. The vertical line marks the time when the bubble attains the theoretical maximum volume V_{max}. The curve corresponds to the curve in figure 21 but redrawn to an equivalent timescale: $\mathrm{d}V/\mathrm{d}t = \text{constant} = 4.00$. There is a fairly close agreement, showing that the increase in volume was uniform in time.

From figure 22, the limiting volume is reached at a time $t = -75$ ms. Thereafter, the motion is dynamic. (A simple analogy is the falling of a rectangular block when it is pushed gently over the edge of a table.) The height H of the bubble continues to rise, but its maximum width $2y_{max}$ stays almost constant, as seen in figure 23. On
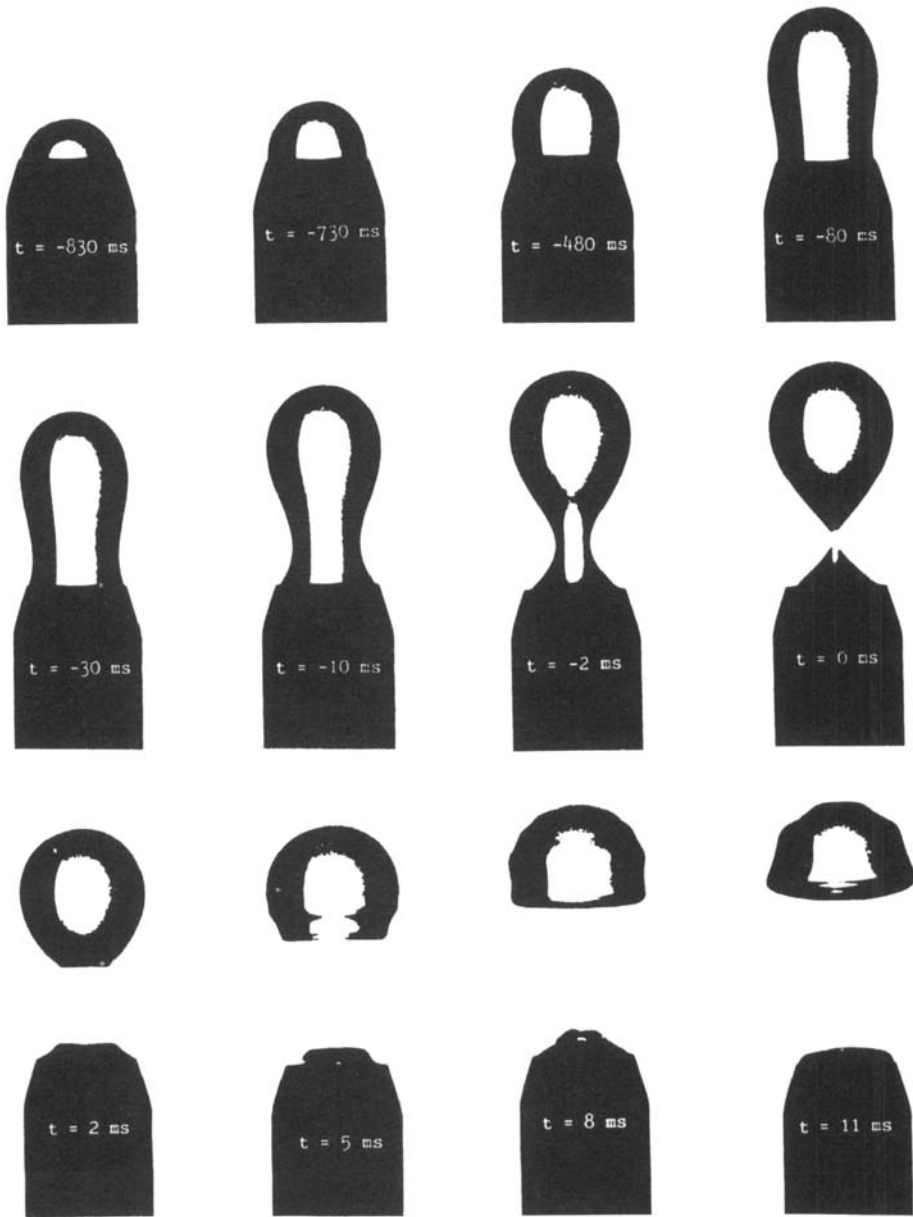
FIGURE 19. A bubble emerging from an underwater nozzle of internal diameter 4.00 mm at a rate of about 1 bubble/s. Film speed: 2000 frames/s.

the other hand the minimum width $2y_{min}$ falls steeply to zero; see the middle curve in figure 23.

We may interpret these results as follows. The motion of the water can presumably be described as due to a continuous distribution of sources and sinks along the vertical axis of the bubble cavity. Consider then the behaviour of y_{min} as a function of the time. If $S(z, t)$ denotes the strength of the sink per unit distance z, then close to the axis we have
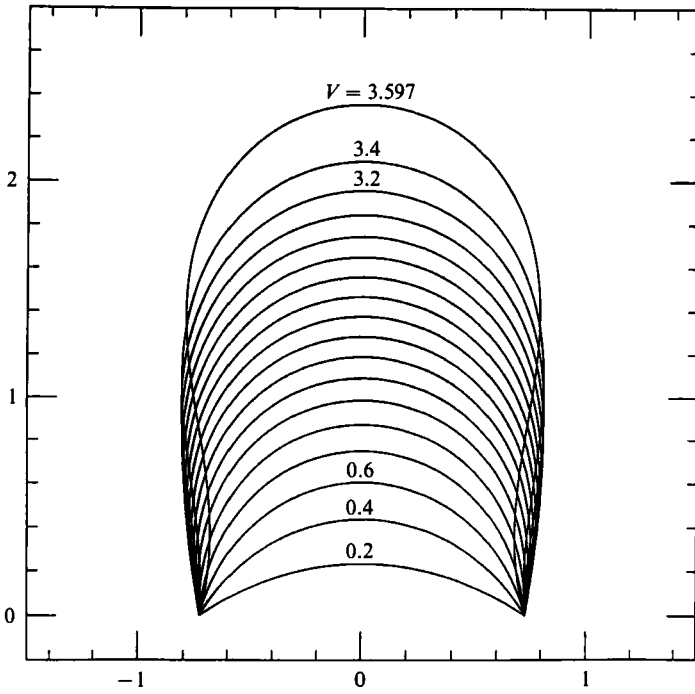
$$\frac{d}{dt}(\pi y_{min}^2) = -S. \tag{9.1}$$

FIGURE 20. Theoretical bubble profiles for a nozzle of dimensionless diameter $D = 1.456$, with constant increment of volume V.
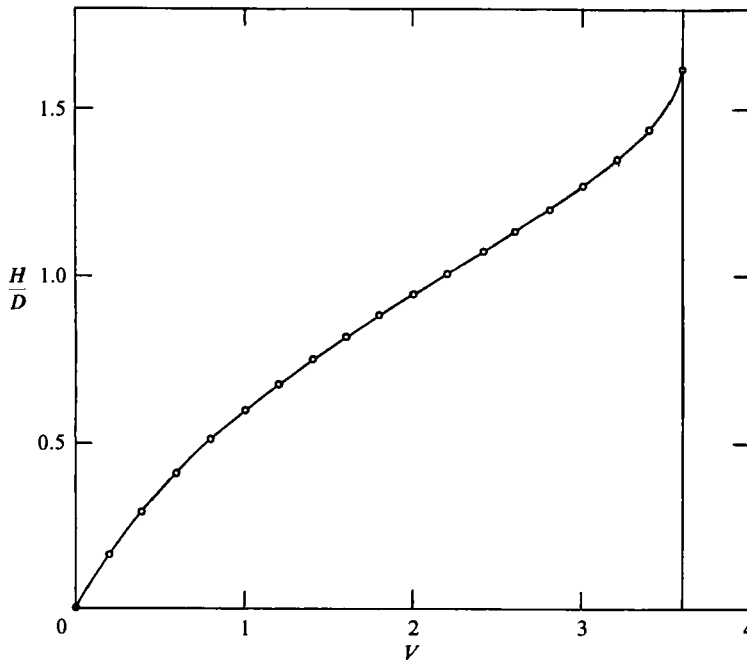

FIGURE 21. Ratio of the bubble height H to the nozzle diameter D as a function of the volume V, when $D = 1.456$ (figure 19).
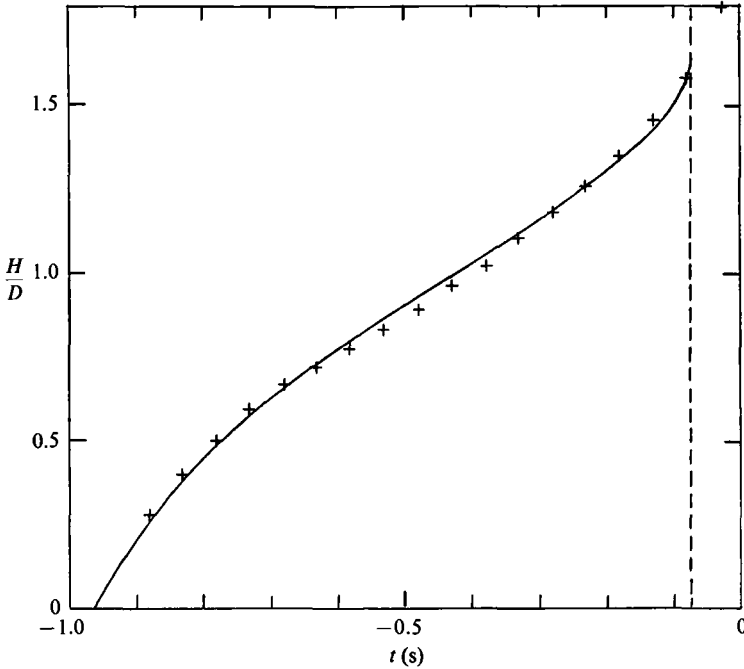
FIGURE 22. Ratio of bubble height H to nozzle diameter D as a function of time. Crosses: observations from figure 18. Curve: from figure 21 with constant rate dV/dt.

So if S is a smooth function of t,

$$\pi y_{\min}^2 \sim (t_0 - t) S(z, t_0), \tag{9.2}$$

where $t = t_0$ denotes the instant when the neck closes. Hence $y_{\min}$ behaves like $(t_0 - t)^{\frac{1}{2}}$, whereas $y_{\min}^2$ behaves linearly with t. This is confirmed by the form of the two lower curves in figure 23.

A further consequence of the model is to demonstrate the limiting form of the surface as $t \to t_0$. For in the neighbourhood of the singularity we have for any point y on the free surface

$$y^2 = [t_p(z) - t] S/\pi, \tag{9.3}$$

where $t_p(z)$ is the time at which that fluid particle would meet the axis. At the singularity itself, choose $z = 0$. Then in general

$$t_p(z) = t_0 + Az + Bz^2 + \ldots, \tag{9.4}$$

where A and B are constants. Now t_0 is by hypothesis the earliest time at which a particle meets the axis, so $t_p \geqslant t_0$ for all z. Hence in (9.4) A vanishes and B is positive. At the critical instant, $t = t_p = t_0$ and so from (9.3) to (9.4)

$$y^2 = (BS/\pi) z^2. \tag{9.5}$$

Thus the limiting surface is a cone, with generators $y = \pm (BS/\pi)^{\frac{1}{2}} z$. The conical form is verified by the observed surface profile shown in figure 19 when $t = 0$.

At general times t the profile is given asymptotically by
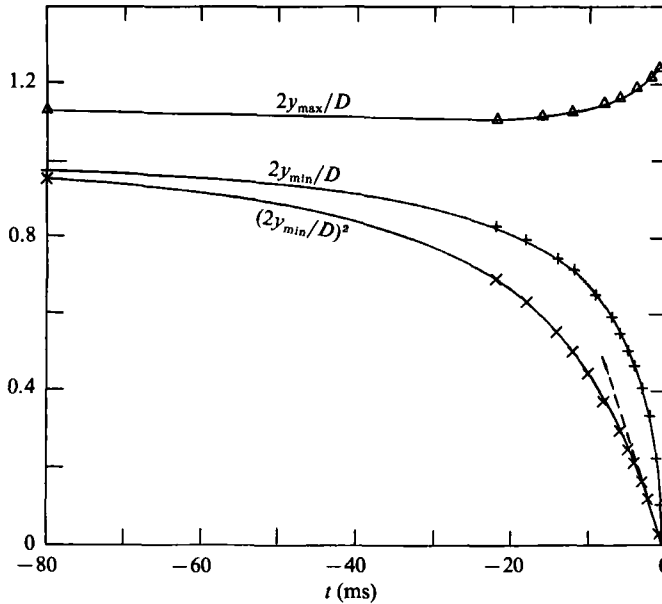
$$y^2 = [(t_0 - t) + Bz^2] S/\pi, \tag{9.6}$$

FIGURE 23. Dimensions of the bubble sequence in figure 19, plotted as functions of the time t.
(a) $2y_{max}/D$, (b) $2y_{min}/D$, (c) $(2y_{min}/D)^2$.

which is a hyperbola. The principal curvature κ_1 of the surface in the axial plane is given by

$$\kappa_1 = -\left(\frac{\partial^2 y}{\partial z^2}\right)_{z=0} = -B\left[\frac{S/\pi}{t_0-t}\right]^{\frac{1}{2}} \tag{9.7}$$

which behaves like $(t_0-t)^{-\frac{1}{2}}$. The other principal curvature is

$$\kappa_2 = (1/y)_{z=0} = [(t_0-t)\,S/\pi]^{-\frac{1}{2}} \tag{9.8}$$

which also behaves like $(t_0-t)^{-\frac{1}{2}}$. The mean curvature $(\kappa_1+\kappa_2)$ remains finite only if

$$BS/\pi = 1, \tag{9.9}$$

that is to say if the generators to the limiting cone make angles of 45° with the axis of symmetry. In other cases, surface tension forces will be important locally though for a short time. In figure 19 the semi-angle of the limiting cone is about 38°.

From figure 23, the bubble neck appears to pinch-off at around $t = t_0 = -0.3$ ms. At $t = 0$ and subsequently there is already evidence of a strong axial jet directed upwards into the bubble, and an opposite jet directed downwards into the nozzle. These jets presumably are required by continuity of mass to compensate for the inflow towards the axis. The calculation of the fluid flows in the jets, and their contribution towards the production of sound by the bubble, is left for a future investigation.

Appendix A. Discussion of experimental errors

We shall consider some possible sources of error for the plotted points in figure 15. The frequency f was based on the simplified expression

$$f = \frac{(3\gamma p_A)^{\frac{1}{2}}}{2\pi a}, \qquad (A\ 1)$$

where p_A denotes the ambient pressure at a depth of 1 m and $\gamma = 1.4$. Since the depth was 72 cm, p_A should be reduced by 2.75% approximately, leading to a reduction in f of 1.4%.

Secondly the assumed value of γ corresponds to adiabatic conditions, and is strictly applicable only to large bubbles. The effect of thermal diffusion is to replace γ in (A 1) by an equivalent quantity η lying between 1.4 and 1.0. In Appendix B below it is shown that the consequent reduction in f, for the bubble sizes under consideration, is given by the approximate formula

$$\Delta f = -0.0072 f^{\frac{3}{2}}, \qquad (A\ 2)$$

where f is measured in kHz. Thus in figure 15, when $D = 0.3\,\text{mm}$, $\Delta f/f$ is about 3.7%, falling to 1% when $D = 6\,\text{mm}$.

A third kind of adjustment arises from the non-sphericity of the bubbles. A bubble in the form of an oblate spheroid was shown by Strasberg (1953) to have a slightly increased frequency Δf compared to a sphere of the same volume. This is given by

$$\frac{\Delta f}{f} = e^{-\frac{1}{3}} \left[\frac{(e^2 - 1)^{\frac{1}{2}}}{\arctan (e^2 - 1)^{\frac{1}{2}}} \right]^{\frac{1}{2}} - 1, \qquad (A\ 3)$$

where e is the ratio of the greatest to the least axis of the spheroid. When e is near 1, (A 1) becomes

$$\frac{\Delta f}{f} = \tfrac{2}{45}(e-1)^2 \qquad (A\ 4)$$

very nearly. For a prolate spheroid a similar formula will apply. This correction is positive, and so is of opposite sign to the other two.

Since the decay time of the acoustical pulse as shown for example in figure 16(a) is short compared to the period of the lowest shape oscillation, we may take as a representative value of e that corresponding to the limiting bubble shape at the instant of breakaway. An examination of the limiting shapes in figure 10 shows that the maximum value of e is 1.37, occurring when $D = 0.6$. Thus we estimate that the greatest value of $\Delta f/f$ from this source would be about 0.5%.

Appendix B. Thermal damping

The thermal damping of a radially oscillating bubble arises mainly from a thermal boundary layer of thickness

$$\Delta = (D_1/2\omega)^{\frac{1}{2}}, \qquad (B\ 1)$$

where D_1 is the thermal diffusivity of the air in the bubble and ω is the radian frequency of the oscillation. The thinness of this layer in relation to the bubble radius a is expressed by the ratio

$$X = a/\Delta. \qquad (B\ 2)$$

The resonant frequency ω_0 is given by

$$\omega_0^2 = \frac{3\eta p_0}{a^2},$$ (B 3)

where for large values of X the parameter η takes the adiabatic value $\gamma = 1.4$. In general, η is given by

$$\eta = \frac{\gamma}{1 + d_{\mathrm{TH}}^2}\left[1 + \frac{3(\gamma - 1)}{X}\frac{\sinh X - \sin X}{\cosh X - \cos X}\right]^{-1},$$ (B 4)

where $$d_{\mathrm{TH}} = 3(\gamma - 1)\frac{X(\sinh X + \sin X) - 2(\cosh X - \cos X)}{X^2(\cosh X - \cos X) + 3(\gamma - 1)X(\sinh X - \sin X)},$$ (B 5)

see Eller (1970). For large values of X it is easy to see that

$$d_{\mathrm{TH}} = \frac{3(\gamma - 1)}{X} \ll 1$$ (B 6)

and hence $$\eta = \gamma - \left[\frac{1 - 3(\gamma - 1)}{X}\right].$$ (B 7)

On the other hand when X is small, we find

$$d_{\mathrm{TH}} = \frac{1}{30}\frac{\gamma - 1}{\gamma}X^2$$ (B 8)

and hence $$\eta = 1 + O(X^4).$$ (B 9)

For air we may take $D_1 = 0.2 \text{ cm}^2 \text{ s}^{-1}$. For a bubble of radius $a = 1$ mm we have $f = 3.26$ kHz approximately so that Δ from (B 1) is about 0.022 mm. Hence $X = 45.2$ and for this and all larger bubble sizes we may apply (B 7). Hence the frequency f is slightly reduced in the ratio

$$(\eta/\gamma)^{\frac{1}{2}} = 1 - 0.6(\Delta/a) = 1 - 0.013.$$ (B 10)

Since Δ and a vary as $f^{\frac{1}{2}}$ and f^{-1} respectively, Δ/a varies as $f^{\frac{3}{2}}$. Hence there is a proportional correction Δf to the frequency given approximately by

$$\frac{\Delta f}{f} = -0.013\left(\frac{f}{3.26}\right)^{\frac{3}{2}},$$ (B 11)

f being measured in kHz. Alternatively we can write

$$\Delta f = -0.0072 f^{\frac{5}{2}}.$$ (B 12)

REFERENCES

BASHFORTH, F. & ADAMS, J. C. 1883 *An Attempt to Test the Theories of Capillary Action by Measuring the Theoretical and Measured Forms of Drops of Fluid.* Cambridge University Press, 80 pp. + tables I–IV.

BLANCHARD, D. C. & SYZDEK, L. D. 1977 Production of air bubbles of a specified size. *Chem. Engng Sci.* **32**, 1109–1112.

CLIFT, R., GRACE, J. R. & WEBER, M. E. 1978 *Bubbles, Drops and Particles.* Academic, 380 pp.

DELAUNAY, C. 1841 Sur la surface de révolution dont la courbure moyenne est constante. *J. Math. Pures Appl.* **6**, 309–320.

ELLER, A. I. 1970 Damping constants of pulsating bubbles. *J. Acoust. Soc. Am.* **47**, 1469–1470.

EELLS, J. 1987 The surfaces of Delaunay. *Math. Intelligencer* **9**, 53–57.

FARMER, D. M. & VAGLE, S. 1988 Observations of high-frequency ambient sound generated by wind. In *Sea Surface Sound* (ed. B. R. Kerman), pp. 403–415. Kluwer. 639 pp.

FITZPATRICK, H. M. & STRASBERG, M. 1957 Hydrodynamic sources of sound. In *Proc. 1st Symp. on Naval Hydrodynamics, Washington, D.C. NAS-NRC Publ.* 515, pp. 241–280. Washington: US Govt Printing Office.

FRIZELL, K. W. & ARNDT, R. E. A. 1987 Noise generation by air bubbles in water: an experimental study of creation and splitting. *University of Minnesota, St Anthony Falls Hydraulic Laboratory, Rep.* 269, December 1987, 49 pp.

LEIGHTON, T. G. & WALTON, A. J. 1987 An experimental study of the sound emitted from gas bubbles in a liquid. *Eur. J. Phys.* **8**, 98–104.

LONGUET-HIGGINS, M. S. 1989*a* Monopole emission of sound by asymmetric bubble oscillations. Part 1. Normal modes. *J. Fluid Mech.* **201**, 525–541.

LONGUET-HIGGINS, M. S. 1989*b* Monopole emission of sound by asymmetric bubble oscillations. Part 2. An initial value problem. *J. Fluid Mech.* **201**, 543–565.

LONGUET-HIGGINS, M. S. 1990*a* Bubble noise spectra. *J. Acoust. Soc. Am.* **87**, 652–661.

LONGUET-HIGGINS, M. S. 1990*b* An analytic model of sound production by raindrops. *J. Fluid Mech.* **214**, 395–410.

LUNDE, K. 1991 Ph.D. thesis, University of Cambridge, England.

MEDWIN, H. & BEAKY, M. M. 1989 Bubble sources of the Knudsen sea noise spectra. *J. Acoust. Soc. Am.* **86**, 1124–1130.

MICHAEL, D. H. 1981 Meniscus stability. *Ann. Rev. Fluid Mech.* **13**, 189–215.

MINNAERT, M. 1933 On musical air bubbles and the sounds of running water. *Phil. Mag.* **16**, 235–248.

OĞUZ, H. N. & PROSPERETTI, A. 1991 Numerical calculation of the underwater noise of rain. *J. Fluid Mech.* (to appear).

PADDAY, J. F. 1971 The profiles of axially symmetric menisci. *Phil. Trans. R. Soc. Lond.* A **269**, 265–293.

PADDAY, J. F. & PITT, A. R. 1973 The stability of axisymmetric menisci. *Phil. Trans. R. Soc. Lond.* A **275**, 489–527.

PITTS, E. 1974 The stability of pendant liquid drops. Part 2. Axial symmetry. *J. Fluid Mech.* **63**, 487–508.

PLATEAU, J. 1873 *Statique Expérimentale et Théorique des Liquides Soumis aux Seules Forces Moléculaires*. Gauthiers-Villar, 495 pp.

PLESSET, M. S. & PROSPERETTI, A. 1977 Bubble dynamics and cavitation. *Ann. Rev. Fluid Mech.* **9**, 145–185.

PROSPERETTI, A., CRUM, L. A. & PUMPHREY, H. D. 1989 The underwater noise of rain. *J. Geophys. Res.* **94**, 3255–3259.

STRASBERG, M. 1953 The pulsation frequency of nonspherical gas bubbles in liquids. *J. Acoust. Soc. Am.* **25**, 536–537.

STRASBERG, M. 1956 Gas bubbles as sources of sound in liquids. *J. Acoust. Soc. Am.* **28**, 20–26.

UPDEGRAFF, G. E. 1989 In situ investigation of sea surface noise from a depth of one meter. Ph.D. dissertation, University of California, San Diego, 223 pp.